Available online at www.sciencedirect.com
SCIENCE DIRECT®
Journal of Non-Crystalline Solids 351 (2005) 2425–2432
JOURNAL OF NON-CRYSTALLINE SOLIDS
www.elsevier.com/locate/jnoncrysol

The effect of Cs_2O additions on HLW wasteform glasses

B.G. Parkinson [a], D. Holland [a,*], M.E. Smith [a], A.P. Howes [a], C.R. Scales [b]

[a] *Department of Physics, Warwick University, Coventry CV4 7AL, UK*
[b] *British Nuclear Fuels Ltd., Sellafield, Seascale, Cumbria CA20 8PG, UK*

Received 7 April 2005; received in revised form 10 June 2005

Abstract

Physical parameters and structural characteristics are reported for the mixed alkali borosilicate glass system, $xCs_2O(100-x)$(MW) ($0 \leqslant x \leqslant 9.66$) where MW is the BNFL wasteform glass (10.29 mol% Li_2O, 10.53 mol% Na_2O, 18.57 mol% B_2O_3, 60.61 mol% SiO_2). Glass density was found to increase with x whilst the glass transition temperature (T_g) decreased. The fraction of four-coordinated boron (N_4) determined from ^{11}B magic angle spinning nuclear magnetic resonance (MAS NMR) increased with x in a manner consistent with previous reports on the sodium–lithium–borosilicate system and contrary to the Dell model. ^{29}Si MAS NMR was used to identify the fraction of Q^4 (B) and Q^3 units as a function of x. Raman spectra indicated the presence of reedmergnerite and danburite superstructural units. Mass loss measurements showed a non-linear variation with x, having a maximum between 7 and 8 mol% Cs_2O and a correlation was found between the amount of Q^3 units in the solid and the volatilization loss from the melt.

PACS: 61.43.F; 61.18.F; 28.41.k; 78.30

1. Introduction

A mixed alkali borosilicate glass of composition 10.29 mol% Li_2O, 10.53 mol% Na_2O, 18.57 mol% B_2O_3, 60.61 mol% SiO_2, is currently used as a wasteform for the vitrification of high level nuclear waste (HLW) [1–3]. A significant problem associated with the process is the evolution of a volatile species at the glass melt stage. Although the volatile species is known [4] to be cesium-containing, its overall composition and the conditions controlling its formation have still to be established. We have sought to identify those structural changes which occur in the solid glass when Cs_2O is added to the wasteform and attempt to relate these to the measured volatilization losses from the melt.

Many studies have been made of borosilicate glasses using MAS NMR, Raman spectroscopy and thermal analysis techniques [5–21]. These have focused on variations in the structure of the borate and silicate glass networks, as a function of alkali content, which lead to changes in density and thermal character.

Structural studies, using ^{11}B, ^{29}Si and ^{17}O magic angle spinning nuclear magnetic resonance (MAS NMR), have led to widely accepted models for both the borate and borosilicate systems [5–19]. The addition of a glass modifier to a borate/borosilicate glass network initially converts trigonal planar, three-coordinated boron in $[BO_3]$ units (B_3) to tetrahedral, four-coordinated boron in $[BO_4]^-$ units (B_4). At higher modifier concentrations, B_4 are replaced by B_3^- i.e. trigonal planar borons with one non-bridging oxygen (NBO) [5,6]. The trend in the fraction of four-coordinated boron (N_4) differs between the borate and borosilicate glass systems although both are non-linear in nature. The most accurate N_4 model to date for the borosilicate glass system is that of Dell et al.

* Corresponding author. Tel.: +44 203 523396; fax: +44 203 692016.
E-mail address: d.holland@warwick.ac.uk (D. Holland).

0022-3093/$ - see front matter © 2005 Elsevier B.V. All rights reserved.
doi:10.1016/j.jnoncrysol.2005.06.035

[7] although recently ^{11}B NMR measurements [8] have shown this model to be incorrect for $R > 0.5$, where R is the ratio of alkali oxide to boron oxide content. ^{29}Si MAS NMR of borosilicate glasses has enabled the identification of the Q^n fractions (n denoting the number of bridging oxygens). Most commonly these are observed as Q^4, Q^3 and Q^4 (B) units, where (B) indicates $3Si + 1B$ next nearest neighbors. Q^2 sites are only possible when there is sufficient alkali oxide associated with the silicate network that the ratio of alkali oxide to silica exceeds 1:2. Raman spectroscopy has been used to detect superstructural units in alkali borate glasses which relate to those seen in the corresponding crystals [20]. However, limited work has been carried out on alkali borosilicate glass systems [21]. This study aims to provide an understanding of how volatility is affected by cesium oxide concentration by identifying changes in the types and fractions of silicon and boron units using ^{11}B and ^{29}Si MAS NMR, and Raman spectroscopy, as well as highlighting changes in thermal behavior as a function of composition.

2. Experimental

2.1. Sample preparation and physical property measurements

Six mixed alkali borosilicate glasses (Table 1) were made at compositions $xCs_2O(100 - x)MW$, ($x = 0$, 2.42, 3.62, 4.83, 7.25 and 9.66), where MW represents the sodium oxide–lithium oxide–borosilicate base glass used by BNFL Ltd. to vitrify HLW. One hundred gram batches were made with reagent grade lithium carbonate (99.9%), sodium carbonate (99.95%), sodium tetraborate (99.5%) and Wacomsil© quartz (99.9%) with 0.1 mol% iron (III) oxide (99.5%) added to reduce NMR T_1 relaxation times. Samples were mixed on rollers for 24 h before being transferred to 90%Pt/10%Rh crucibles and heated to between 1350 °C and 1400 °C (depending on composition) for 20 min before being cast into de-ionized water to form a frit. Samples were then re-melted at the same temperature, cast and annealed at 50 °C below the glass transition temperature, measured from the frit using DTA. Samples were analyzed with X-ray diffraction (XRD) to confirm their amorphous character.

Table 1
Nominal compositions of the glasses (mol%)

Cs_2O	Li_2O	Na_2O	B_2O_3	SiO_2
0	10.29	10.53	18.570	60.610
2.42	10.041	10.275	18.121	59.143
3.62	9.918	10.149	17.898	58.416
4.83	9.793	10.021	17.673	57.683
7.25	9.544	9.767	17.224	56.216
9.66	9.296	9.513	16.776	54.755

Differential thermal analysis (DTA) was carried out with approximately 0.2 g of each sample ground and loaded into a 90%Pt/10%Rh crucible. Samples were heated at 10 °C/min to 1000 °C, in air, in a Stanton-Redcroft DTA 673-4 with a quartz reference.

Density measurements were made using the Archimedes method, with glycerol being used as the displacement fluid to avoid moisture attack on the high alkali-content glasses.

2.2. Nuclear magnetic resonance

^{133}Cs MAS NMR spectra were obtained using a Varian Infinity 360 NMR spectrometer operating at 47.24 MHz with a Doty MAS 4 mm probe spinning at 10 kHz. A one pulse program was used with a pulse delay of 5 s, a 1.3 μs pulse width ($B_1 \sim 67$ kHz) and 1000 acquisitions. Samples were referenced against solid CsCl taken as 223.2 ppm, with respect to the primary reference of 1 M aqueous CsCl. ^{11}B MAS NMR spectra were obtained on a Varian/Chemagnetics Infinity 600 NMR spectrometer operating at 192.04 MHz with a Chemagnetics MAS 4 mm probe spinning at 15 kHz. For each sample 1000 acquisitions were taken with a pulse delay of 1 s and a 0.7 μs pulse width ($B_1 \sim$ 60 kHz). Samples were referenced against BPO_4 solid taken as −3.3 ppm with respect to the primary reference $Et_2O{:}BF_3$ at 0 ppm. ^{29}Si MAS NMR was carried out using a CMX Infinity 360 NMR spectrometer operating at 71.25 MHz with a 6 mm probe spinning at 6 kHz. A 5 s pulse delay and 2 μs pulse width (30° tip angle) were used with 1000 acquisitions. Samples were referenced to tetramethylsilane (TMS) at 0 ppm. Peak fits were made using the DMfit2002 NMR program [22].

2.3. Raman spectroscopy

Raman spectra were obtained at room temperature with a Renishaw Invia Raman spectrometer equipped with a 20 mW Argon Laser operating at 514 nm. Measurements reported here were acquired at room temperature with 10 mW incident laser power and a 50× objective. The spectrometer resolution was approximately 2 cm^{-1}.

2.4. Volatilization measurements

Mass loss measurements were made by heating ~0.2 g of sample in a 90%Pt/10%Rh crucible at 1000 °C for 30 min with a heating rate of 10 °C/min. Volatile species were condensed onto an alumina lid placed over the crucible and then subjected to energy dispersive X-ray analysis (EDX) in an EDAX Genesis scanning electron microscope.

3. Results

The samples were amorphous within the limits of detection by XRD. The results from DTA and from density measurements are presented in Table 2. Apart from the glass transition, the DTA traces are featureless, reflecting the stability of these glasses. The values of the glass transition temperature T_g are listed in Table 2 and plotted as a function of x in Fig. 1. The density values are plotted as a function of x in Fig. 2 along with the values for molar volume M_V, calculated from $M_V = M/\rho$ where M is the molar mass of the glass in grams and ρ is the density in g cm^{-3}.

The ^{133}Cs MAS NMR spectra are shown in Fig. 3. There is insufficient detail in the broad, rather Gaussian-like resonances to be able to fit a detailed lineshape, therefore only the peak maximum positions and half widths are reported (Table 3). The position of the peak maximum was observed to increase approximately linearly with Cs_2O content (Fig. 4). ^{133}Cs is a quadrupole nucleus which might be expected to produce asymmetric lines from the residual second-order quadrupolar broadening of a distribution of quadrupole interactions [23].

Table 2
Densities, molar volumes and glass transition temperatures for the cesium oxide–base glass system

Cs_2O (mol%)	Density (±0.07 g/cm^3)	Molar volume (±0.9 cm^3/mol)	T_g (±5 °C)	Mass loss (±0.4%)
0	2.32	26.4	494	0
2.42	2.40	26.8	478	0.3
3.62	2.52	26.5	467	1.0
4.83	2.47	28.2	463	1.6
7.25	2.62	28.7	454	2.0
9.66	2.65	30.4	453	0.7

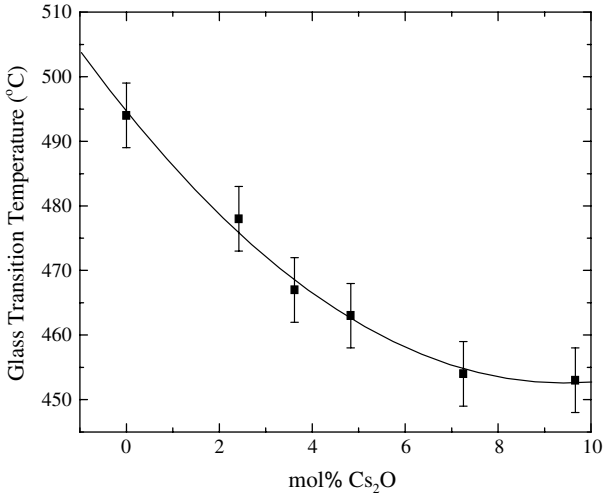

Fig. 1. Glass transition temperatures (T_g) as a function of Cs_2O content for the cesium oxide–sodium oxide–lithium oxide borosilicate glasses.

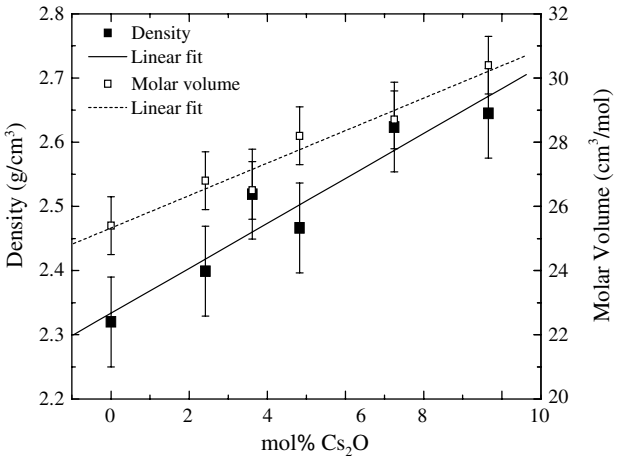

Fig. 2. Density and molar volume (M_V) as a function of Cs_2O content for the cesium oxide–sodium oxide–lithium oxide borosilicate glasses.

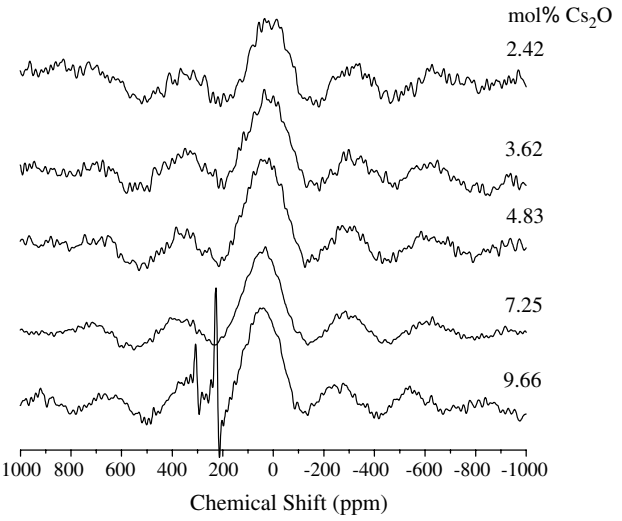

Fig. 3. ^{133}Cs MAS NMR spectra for the cesium oxide–sodium oxide–lithium oxide borosilicate glasses. Sharp peak at +220 ppm is from the CsCl (solid) used as a reference. Origin of peak at 290 ppm is unknown.

Table 3
^{133}Cs MAS NMR peak maximum positions and peak half widths

Cs_2O (mol%)	Position (±5 ppm)	Half width (±5 ppm)
2.42	16	175
3.62	23	183
4.83	34	176
7.25	41	168
9.66	45	172

However, ^{133}Cs has a very small quadrupole moment so that the linewidth is likely to be dominated by chemical shift dispersion which produces a symmetric line. The sharp line observed in the 9.66 mol% Cs_2O spectrum at +210 ppm is from the cesium chloride reference.

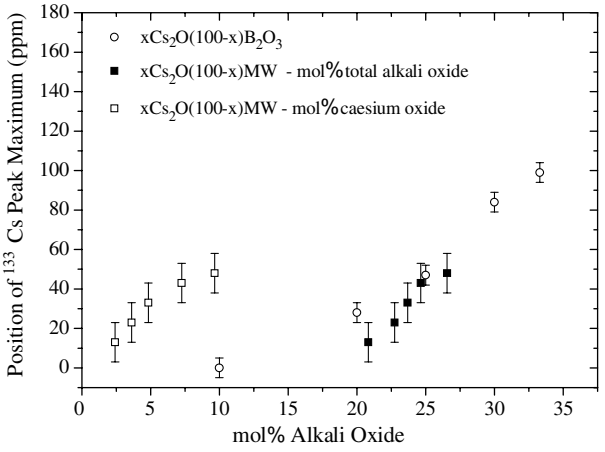

Fig. 4. Peak maximum position of ^{133}Cs MAS NMR spectra as a function of cesium oxide content and total alkali oxide content for the cesium oxide–sodium oxide–lithium oxide borosilicate glasses.

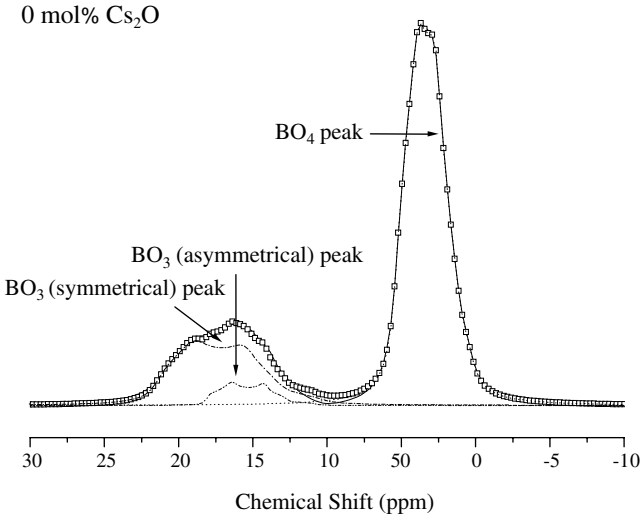

Fig. 6. Typical ^{11}B MAS NMR spectral peak fit for a cesium oxide–sodium oxide–lithium oxide borosilicate glass.

The origin of the second sharp line at +290 ppm is unknown but it does not interfere with the main lineshape from the glass.

The ^{11}B MAS NMR spectra (Fig. 5) show a large, relatively narrow peak from $[BO_4]$ at ~2.5 ppm and a small broader peak from $[BO_3]$ at ~17 ppm. N_4 values were calculated from resolved peak areas obtained from the DMfit2002 NMR peak fitting program [22]. Spectra were fitted with three peaks; one symmetric and one asymmetric $[BO_3]$ peak and a single symmetric $[BO_4]$ peak. A typical fit is shown in Fig. 6. N_4 values were corrected with the resolved $[BO_3]$ fraction being increased by 4%. This increase is necessary due to the loss, under MAS, of central (1/2, −1/2) transition intensity from the $[BO_3]$ centerband into the spinning sidebands. This does not happen for the $[BO_4]^-$ sites with their much smaller quadrupole interaction so that all of the central (1/2, −1/2) transition intensity appears in the centerband [24].

The ^{29}Si MAS NMR spectra (Fig. 7) were fitted with four Gaussian lines: two Q^3-MAS sideband peaks; one Q^3 peak constrained to be equidistant between the two Q^3-MAS sideband peaks; and one Q^4 (B) peak, a silicon with 3 Si and 1 B next nearest neighbors. Contributions from units with fewer than 3 bridging oxygens were assumed not to exist due to insufficient alkali content. A typical fit is shown in Fig. 8. Resolved Q^3 fractions were observed to increase non-linearly (between 0.55 and 0.88) across the range of compositions, with a maximum

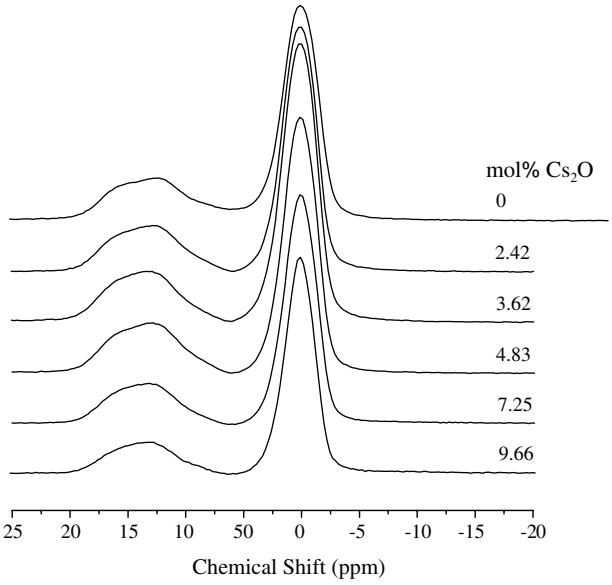

Fig. 5. ^{11}B MAS NMR spectra for the cesium oxide–sodium oxide–lithium oxide borosilicate glasses.

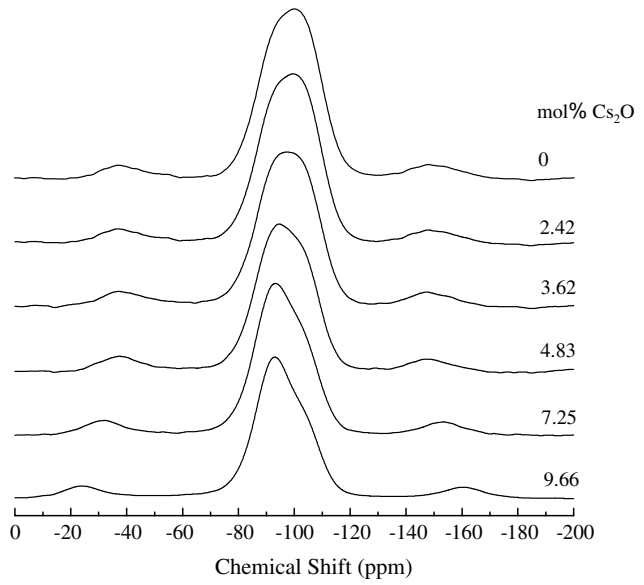

Fig. 7. ^{29}Si MAS NMR spectra for the cesium oxide–sodium oxide–lithium oxide borosilicate glasses.

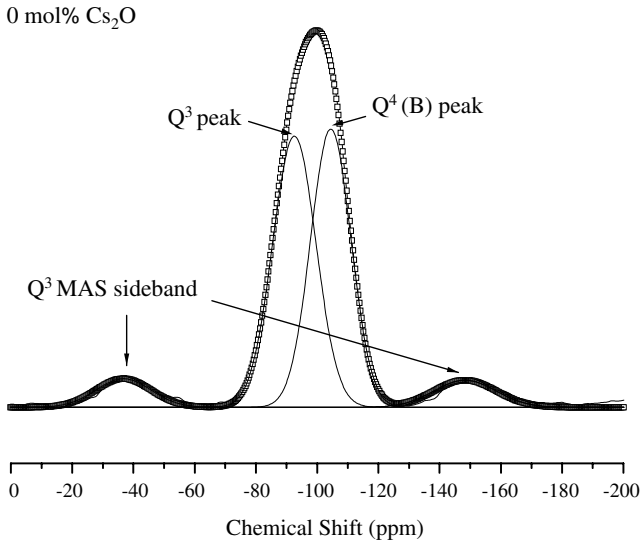

Fig. 8. Typical ^{29}Si MAS NMR spectral fit for a cesium oxide–sodium oxide–lithium oxide borosilicate glass.

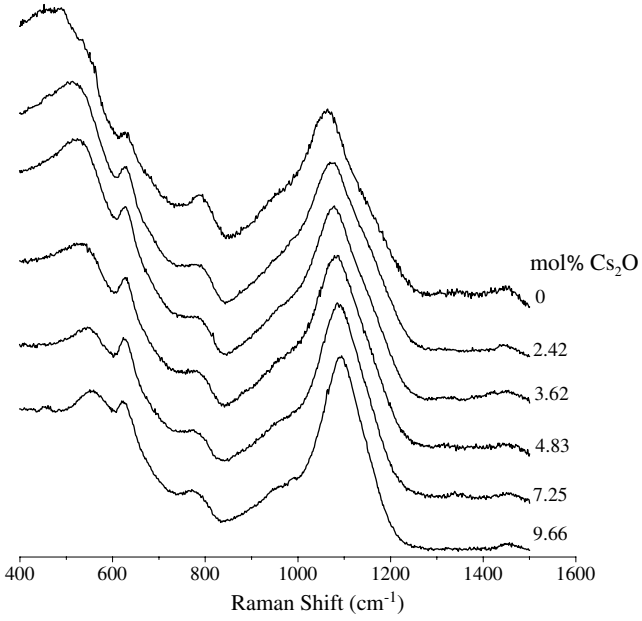

Fig. 9. Raman spectra for the cesium oxide–sodium oxide–lithium oxide borosilicate glasses.

at 7.25 mol% Cs_2O (Table 4). This was mirrored by a non-linear decrease in the fraction of Q^4 (B) units.

The Raman spectra from the cesium-mixed alkali borosilicate glasses are shown in Fig. 9. Baseline corrections were made to all data such as to give a horizontal baseline above 1200 cm^{-1}. A typical fit to a Raman spectrum using Gaussian peak shapes is shown in Fig. 10.

Mass loss values for the samples are presented in Table 2 and a typical EDX spectrum from the deposit is shown in Fig. 11. This shows that, in addition to cesium, silicon and sodium are also present in the deposit. Light elements such as lithium and boron are not easily detectable by EDX.

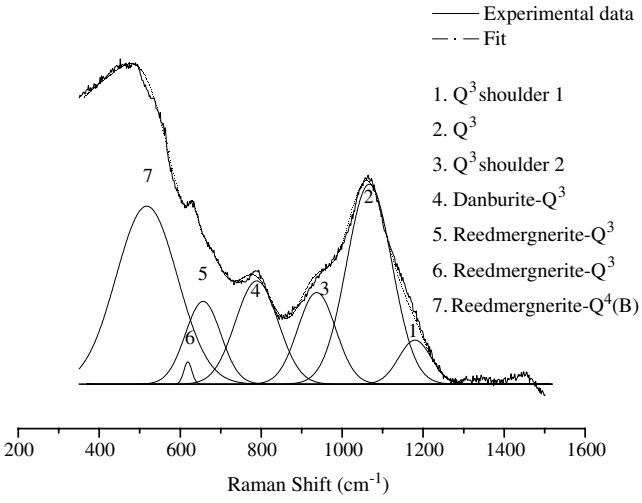

Fig. 10. Typical Raman plot (3.62 mol% Cs_2O glass composition) of resolved peaks.

4. Discussion

The decrease in T_g with x (Fig. 1) is consistent with the increase in modifier in the system though N_4 also increases (see below), which can produce an increase in T_g as a consequence of increased network connectivity. An additional factor may be the reduced heat of formation for cesium oxide (−345.8 kJ/mol) compared to the other two alkali oxides present (sodium oxide, −414 kJ/mol, lithium oxide, −597.9 kJ/mol) indicating weaker bonds.

Table 4
Positions, half-widths and fractions for the resolved ^{29}Si MAS NMR peaks

Cs_2O (mol%)	Q^3			Q^4 (B)		
	δ (±0.5 ppm)	Δ (±1 ppm)	Resolved fraction	δ (±0.5 ppm)	Δ (±1 ppm)	Resolved fraction
0	−92.4	17	0.57 ± 0.07	−104.5	16	0.43 ± 0.07
2.42	−92.1	18	0.57 ± 0.04	−104.2	17	0.43 ± 0.04
3.62	−91.9	18	0.59 ± 0.04	−103.8	16	0.41 ± 0.04
4.83	−91.9	17	0.66 ± 0.04	−103.8	16	0.36 ± 0.04
7.25	−92.6	17	0.79 ± 0.04	−105.1	14	0.19 ± 0.04
9.66	−91.7	16	0.71 ± 0.07	−103.8	13	0.29 ± 0.02

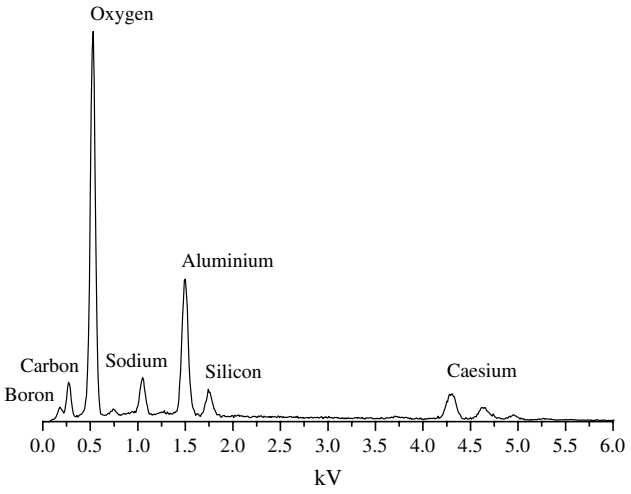

Fig. 11. EDX spectrum of a deposit collected from the 7.25 mol% Cs_2O glass volatilization experiment.

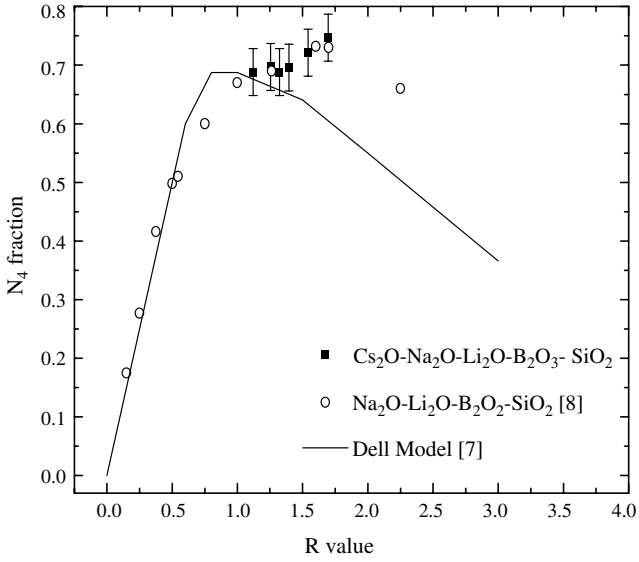

Fig. 12. ^{11}B MAS NMR N_4 fractions for cesium oxide–sodium oxide–lithium oxide borosilicate ($K = 3.2$), sodium oxide–lithium oxide borosilicate glasses [8] ($K = 3.0$) and the Dell model [7] ($K = 3.0$).

The linear increase in density (Fig. 2) is a consequence of the dominating cesium oxide density (4.25 g/cm^3 compared to 2.27 (Na_2O), 2.01 (Li_2O), 2.65 (SiO_2) and 2.46 (c-B_2O_3)). The molar volume also increases linearly with cesium oxide content, with the glass having to expand to accommodate the insertion of large Cs^+ ions into the limited space available.

The linear change of peak maximum with Cs_2O content in Fig. 4 is a trend common to all alkalis in borate glasses [25]. If the positions are plotted against total alkali oxide content and compared with the values obtained for binary cesium borate glasses, then it can be seen that there is little effect from the type of alkali ion or indeed the network. This trend is due to reduction in shielding, suggesting increasing charge transfer to the network by whatever alkali ions are present.

The change in N_4 fraction with R, the ratio of total mol% alkali oxide to mol% boron oxide content, is shown in Fig. 12 and compared with values obtained by Roderick [8] and with the Dell [7] model. It can be seen that there is good agreement (±0.01) with values obtained for the lithium sodium borosilicate glass system [8], for similar compositions. This adds weight to the argument that the value of N_4 is independent of alkali type. Values differ significantly from the Dell model [7] for $R > 0.5$, with the quantity of four-coordinated boron initially being less than predicted and then, when $R > 1.0$, increasing in contrast to the theory, which predicts N_4 should decrease as the result of an increase in Q^3 silicon units.

The Raman peaks in the spectra in Fig. 10 have been identified by comparison with reports by Utegulov et al. [26] and Bunker et al. [21] on the Al_2O–SiO_2–Na_2O–MgO–Eu_2O_3 and Na_2O–SiO_2–B_2O_3 glass systems respectively (Table 5). Peaks due to reedmergnerite (four-membered rings containing three [SiO_4] and one [BO_4]) and danburite (four-membered rings containing two adjacent [SiO_4] and two adjacent [BO_4]) units are observed. Their presence explains the high N_4 values compared to binary borates since the [BO_4] units are stabilized by adjacent [SiO_4] units. The lack of any resolvable Q^2 units in the ^{29}Si MAS NMR data is confirmed with no Q^2 Si–O Raman vibrational mode present at 950 ± 4 cm^{-1}. The positions of both the reedmergnerite-Q^4 (B) and the Q^3 peaks (initially at 489 ± 4 and 1061 ± 4 cm^{-1} respectively) increase as a function of cesium oxide content. The spectrum below approxi-

Table 5
Raman peak positions, assignments and some intensity relations

Cs_2O (mol%)	300–600 (±4 cm^{-1}) Reedmergnerite-Q^4	600–1000 (±4 cm^{-1})		1000–1200 (±4 cm^{-1}) Q^3	Resolved Raman Q^3 fractional intensity	Resolved NMR Q^3 fraction	Ratio of NMR Q^3/Raman Q^3 (±0.2)
		Reedmergnerite	Danburite/Q^4				
0	489	626	791	1061	0.20	0.57	2.9
2.42	515	626	796	1076	0.21	0.57	2.7
3.62	532	626	792	1079	0.21	0.59	2.8
4.83	540	629	792	1085	0.24	0.66	2.8
7.25	546	626	782	1085	0.27	0.79	2.9
9.66	552	623	782	1093	0.29	0.71	2.5

mately 200 cm^{-1} is truncated by equipment filters and so has been ignored in any analysis.

The intensity of the resolved Q^3 peak (~1080 cm^{-1}) is compared with the resolved Q^3 fraction from the ^{29}Si MAS NMR data in Table 5. The ratio of the two fractions is constant in the compositional range studied except for the highest Cs_2O content where the resolved Q^3 fraction from the Raman data is greater than expected. This may be due to the increasing uncertainty in fitting the Raman Q^3 peak because of the increasing importance of peak 3 in Fig. 9. The shoulder of the Q^3 peak (peak 3 at ~920 cm^{-1}) has been identified as a Q^2 peak by Utegulov et al. [26] in an aluminosilicate glass. However, there is no evidence for Q^2 from the ^{29}Si MAS NMR.

Mass loss measurements revealed a non-linear variation with composition which matched that of the resolved Q^3 fraction from ^{29}Si MAS NMR data and the change in certain Raman peaks (Fig. 13). EDX measurements have shown the deposit from the vapor to contain Cs, Na, Si, and B, suggesting the volatilization process is more complex than simple removal of cesium borate. The indication from Raman spectroscopy that there are borosilicate super-structural units present in the solid, of the type $Si_2B_2O_8^{2-}$ and $Si_3BO_8^-$, could explain the complexity of the volatilized species, though this presumes that these species are retained in the melt. It is not clear whether the presence of Cs_2O is a necessary condition for volatilization to occur or whether an increase in any alkali content would produce the same effect. The lower Cs–O bond strength compared with other alkalis may be significant but further work is needed to confirm this and structural studies on the melt are required to establish if the structural units detected in the solid glass are carried over into the melt.

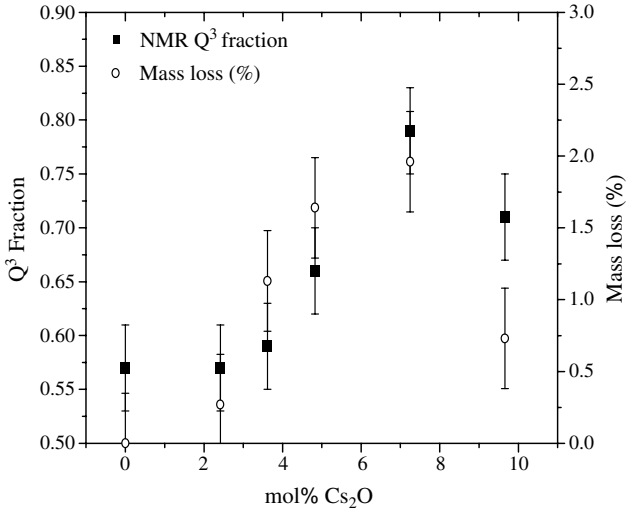

Fig. 13. Resolved ^{29}Si MAS NMR Q^3 fractions and mass loss (%) as a function of Cs_2O content.

5. Conclusions

^{133}Cs MAS NMR measurements have shown these glasses to behave in a similar manner to binary cesium borate glasses with total alkali oxide content being the dominating factor. The N_4 data, ^{29}Si MAS NMR data and Raman spectra presented here do not support the Dell model for the range of xCs$(100 - x)$MW glasses studied. Both the trends in Cs_2O chemical shift and the variation of N_4 values with total alkali content (or R) show that it is the amount of alkali rather than the nature of the alkali which is important. Super-structural units similar to those in reedmergnerite and danburite have been detected with Raman spectroscopy, indicating that the borate and silicate networks are not separated and accounting for the high (~0.7) values of N_4. The ratio of the Q^3 intensity resolved from ^{29}Si MAS NMR to that from Raman spectroscopy for each composition is shown to be constant in the compositional range studied. The dependence of mass loss and hence glass volatility on the fraction of Cs_2O, x, appears to mirror the change from Q^4 (B) to Q^3 units, suggesting a direct link between the formation of non-bridging oxygen sites and glass volatility, although the mechanism may be more complex than this, involving both the reedmergnerite and danburite structural units. Interestingly, the aqueous corrosion of mixed alkali borosilicate glasses has also been shown to be linked to the Q^3 content of the glasses [27].

Acknowledgements

BGP would like to thank British Nuclear Fuels Ltd. for their financial support, EPSRC for partial funding of the NMR facility. Dr Mark Newton and Mr Robin Cruddace are thanked for their help with Raman measurements.

References

[1] M.J. Plodinec, Glass. Tech. 41 (2000) 186.
[2] W.J. Weber, R.C. Ewing, C.A. Angell, G.W. Arnold, A.N. Cormack, J.M. Delaye, D.L. Griscom, L.W. Hobbs, A. Navtrosky, D.L. Price, A.M. Stoneham, M.C. Weinburg, J. Mater. Res. 12 (1997) 1946.
[3] I.W. Donald, B.L. Metcalfe, R.N.J. Taylor, J. Mater. Sci. 32 (1997).
[4] I.Y. Archakov, V.L. Stolyarova, M.M. Shultz, Rapid Commun., Mass Spectrum 12 (1998) 1339.
[5] G.E. Jellison, P.J. Bray, J. Non-Cryst. Solids 29 (1978) 187.
[6] S. Feller, W.J. Dell, P.J. Bray, J. Non-Cryst. Solids 51 (1982) 21.
[7] W.J. Dell, P.J. Bray, S.Z. Xiao, J. Non-Cryst. Solids 58 (1983) 1.
[8] J.M. Roderick, D. Holland, A.P. Howes, C.R. Scales, J. Non-Cryst. Solids 293–295 (2001) 746.
[9] J.M. Roderick, D. Holland, C.R. Scales, Phys. Chem. Glasses 41 (2000) 392.

[10] A. Duddridge, D. Holland, S.M. Dixon, Glass Tech. 44 (2003) 85.
[11] D. Chen, H. Miyoshi, H. Mausi, T. Akai, T. Yazawa, J. Non-Cryst. Solids 345&346 (2004) 104.
[12] B. Luckscheiter, M. Nesovic, Waste Manage. 16 (1996) 571.
[13] T. Furukawa, W.B. White, J. Mater. Sci. 16 (1981) 2689.
[14] L.-S. Du, J.F. Stebbins, J. Non-Cryst. Solids 315 (2003) 239.
[15] L.-S. Du, J.F. Stebbins, J. Phys. Chem. B 107 (2003) 10063.
[16] S.K. Lee, C.B. Musgrave, P. Zhao, J.F. Stebbins, J. Phys. Chem. B 105 (2001) 12583.
[17] P. Zhao, S. Kroeker, J.F. Stebbins, J. Non-Cryst. Solids 276 (2000) 122.
[18] L. van Wüllen, G. Schwering, Solid-State Nucl. Magn. Resn. 21 (2002) 134.
[19] R. Martens, W. Müller-Warmuth, J. Non-Cryst. Solids 265 (2000) 167.
[20] M. Kodama, S. Kojima, Jpn. J. Appl. Phys. 33 (1994) 2886.
[21] B.C. Bunker, D.R. Tallant, R.J. Kirkpatrick, G.L. Turner, Phys. Chem. Glasses 31 (1) (1990).
[22] D. Massiot, F. Fayon, M. Capron, I. King, S. Le Calve, B. Alonso, J.O. Durand, B. Bujoli, Z. Gan, G. Hoatson, Magn. Reson. Chem. 340 (2002) 76.
[23] M.E. Smith, E.R.H. van Eck, Prog. Nucl. Magn. Resn. Spec. 34 (1999) 159.
[24] K.J.D. Mackenzie, M.E. Smith, Multinuclear Solid-State NMR of Inorganic Materials, Pergamon Materials Series, vol. 6, 2002.
[25] E. Ratai, M. Janssen, H. Eckert, Solid State Ionics 105 (1998) 25.
[26] Z.N. Utegulov, J.P. Wiskstead, G.-Q. Shen, Phys. Chem. Glasses 45 (3) (2004) 166.
[27] M.M. Islam, D. Holland, A.P. Howes, C.R. Scales, Phys. Chem. Glasses, in preparation.